

Mechanical characterization of the stainless steel welds for the JT-60SA Cryostat Vessel Body Cylindrical Section

Mercedes Medrano^{a,c,*}, Marta Serrano^b, Rebeca Hernández^b, Daniel Plaza^b, Antonio Muñoz^b, Esther Rincón^a, Santiago Cabrera^a, Alfonso Soletó^a, Augusto Pereira^{a,c}, Cristina Alén^c

^a Laboratorio Nacional de Fusión, CIEMAT, Avda. Complutense 40, 28040 Madrid, Spain

^b División de Materiales de Interés Energético, Departamento de Tecnología, CIEMAT, Avda. Complutense 40, 28040 Madrid, Spain

^c Universidad de Alcalá de Henares, Pza. San Diego, s/n, 28801 - Alcalá de Henares, Madrid, Spain

ARTICLE INFO

Keywords:

JT-60SA
Cryostat
Manufacturing

ABSTRACT

JT-60SA is the superconducting tokamak that will be operated at the Naka Fusion Institute of QST (the National Institutes for Quantum and Radiological Science and Technology) in Japan. The project is being developed under the framework of the Broader Approach Agreement between the EU and Japan (started in 2007) for an early realization of the fusion energy, aimed at conducting supportive and complementary work for the ITER experimental program towards DEMO. The assembly of the tokamak components as well as the related equipment was completed last year and the device is currently undergoing the integrated commissioning phase.

Within the European contribution, Spain was one of the stakeholders that committed it, as a Voluntary Contributor, to design and manufacture one of the main components of the device: the cryostat. The cryostat is a large stainless steel vacuum vessel, 14 m diameter, 16 m high, which encloses the tokamak and provides the vacuum boundary (10^{-3} Pa) necessary to limit the heat loads on the magnets operated at cryogenic temperatures. The component is made up of the Cryostat Base (CB), the Cryostat Vessel Body Cylindrical Section (CVBCS), both designed and fabricated in Spain (through the National Fusion Laboratory at Ciemat), as well as the cryostat top lid (CTL) designed and procured by Japan (through QST).

Within the manufacturing phases of the CB and CVBCS an extensive test program was carried out at Ciemat that focussed on the characterization of the welding processes selected for the manufacturing before their final approval. The aim of this paper is to present the results of the mechanical and microstructural tests performed on the welded joints.

Introduction

JT-60SA is a superconducting tokamak that will be operated at the Naka Fusion Institute of QST (the National Institutes for Quantum and Radiological Science and Technology) in Japan. The goal of the JT-60SA device is to support and complement the ITER experimental program towards supporting the basis for DEMO. The JT-60SA project is being developed under the framework of the Broader Approach Agreement (BA) and the Japanese national fusion programme for an early realization of fusion energy [1]. The manufacturing of the components and plant systems has been shared between the EU and Japan within this Agreement. Within the European contribution, Spain is one of the stakeholders which, as a Voluntary Contributor, was committed to deliver the JT-60SA cryostat. The assembly of the tokamak components

and related equipment, as well as the plant systems, were completed in 2020 and the device is currently undergoing the integrated commissioning phase. A sketch of the device is shown in Fig. 1 and the main parameters are included in Table 1.

The cryostat is a large vessel that encloses the main components of the device, these being the Vacuum Vessel, Toroidal Field coils, Equilibrium Field coils, Central Solenoid modules, etc. It maintains the vacuum boundary needed to limit the heat loads on the magnets operated at cryogenic temperatures from the room temperature (RT) environment. From a functional point of view, the cryostat was divided in different assemblies as it is shown in Fig. 2, i.e.: the Cryostat Base (CB), the Cryostat Vessel Body Cylindrical Section (CVBCS), and the Cryostat Top Lid (TL). Spain through the National Fusion Laboratory at Ciemat provided the CB and CVBCS designs [2,3] and the manufacturing of both

* Corresponding author at: Laboratorio Nacional de Fusión, CIEMAT, Avda. Complutense 40, 28040 Madrid, Spain.

E-mail address: mercedes.medrano@ciemat.es (M. Medrano).

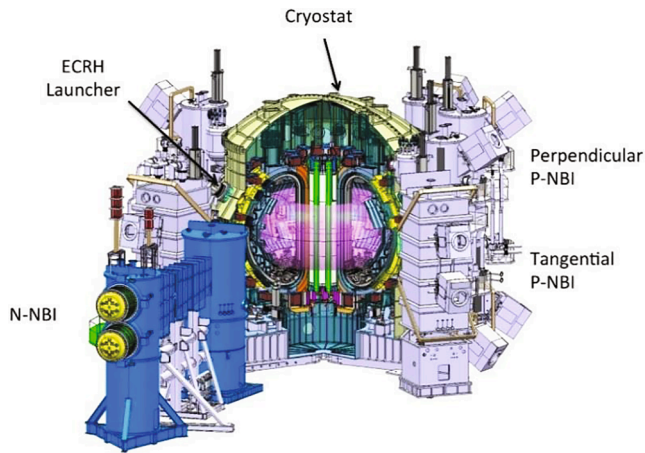


Fig. 1. JT-60SA superconducting Tokamak.

Table 1
JT-60SA main parameters.

Parameter	Value
Plasma current	5.5 MA
Toroidal field	2.25 T
Major radius	2.96 m
Minor radius	1.18
Aspect ratio	2.5
Elongation Kx	1.95
Triangularity	0.53
Flattop duration	100 s
Heating & CD power	41 MW
N-NBI	10 MW
P-NBI	24 MW
ECRF	7 MW

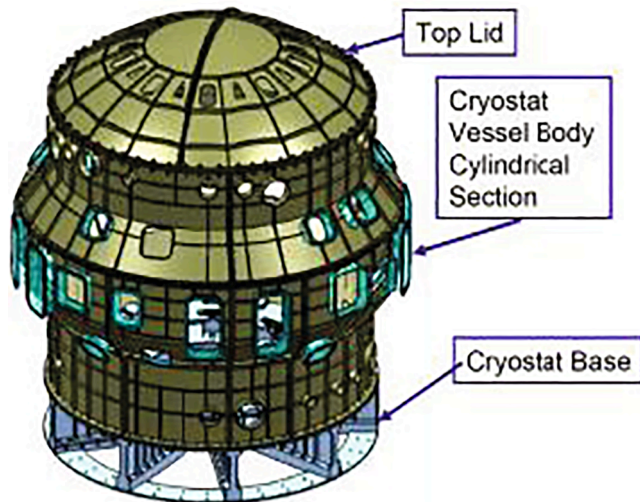


Fig. 2. JT-60SA cryostat.

assemblies [4,5]. In parallel, the TL was delivered by Japan. The main parameters of the cryostat are listed in Table 2.

The CB constitutes a heavy construction with a diameter ~ 12 m, a height of 2.9 m and a weight of ~ 245 ton which must support the weight of all the tokamak components and withstand the loads associated with the operation of the machine transferring all the loads to the tokamak building foundations. The CVBCS supports the weight of all the ports and port plugs as well as the loads originated during the operation of the

Table 2
Main parameters of the JT-60SA cryostat.

JT-60SA cryostat main Parameters	
Overall Cryostat dimensions	ϕ 13.47 m x 15.85 m height
CB dimensions	ϕ 13.47 m x 15.85 m height
CVBCS dimensions	ϕ 13.47 m x 15.85 m height
Volume	1410 m ³
Cryostat/CB/CVBCS weight	468/245/175 ton
Operational pressure	Vacuum, 10 ⁻³ Pa
Surface exposed to vacuum	1368 m ²
Design Temperature	293 K

experiment in normal/abnormal conditions (such us vacuum pressure/ overpressure, electromagnetic loads) or external events (seismic loads). The CVBCS is assembled onto the massive CB while the TL, installed on the upper part, closes the cryostat. The CVBCS is constituted by 12 made up of a single 34 mm thick wall, externally reinforced with 20 mm thick ribs [5]. The total weight is up to ~ 175 ton (see Fig. 3). Each individual sector consists of a fully welded structure where penetrations have been machined precisely onto the shell. The ports are welded to the openings (some of them as large as 2322 mm x 1152 mm) and then machined to achieve the final tolerances. Due to their open geometry, the sectors turned out to be very flexible, with a relatively thin wall and a large number of openings/ports of different dimensions. Strict tolerances had to be kept during the manufacturing of the sectors and therefore, the definition of a thorough welding sequence had to be set up in order to minimize deformations produced during the welding process. The different sectors are fastened to each other by means of bolted flanges. The vacuum-sealing on the integer component is kept by means of non-structural fillet welds performed on site on the bolted flanges. The vacuum-sealing on the integer component is kept by means of non-structural fillet welds performed on site on the bolted flanges.

Within the CVBCS manufacturing phase, an extensive battery of tests was carried out at Ciemat. They were focussed on characterizing the welds proposed by the manufacturer before their final approval. Therefore, the aim of these tests was the validation of the welding process/type of welds before fabrication could begin. The results of the tests performed are presented in the next sections.

Materials and Methods

The selected base material for the fabrication of the CVBCS was austenitic stainless steel base grade 18/9 (UNS S30400) according to the standard ASTM-240 [6] with some specific requirements such as: a) cobalt content, Co < 0.05 wt %; b) magnetic permeability, $\mu_{rel} \leq 1.1$ (measured on the surface); and c) surface finish Ra ≤ 12.5 μ m. The stainless steel was supplied by the Swedish company, Outokumpu, as hot rolled stainless steel plates with thickness ranging from 20 to 100 mm. For the construction of the sectors, full penetration welded joints were extensively done except for the external ribs made with fillet welds. All the welds were produced using gas metal arc welding (GMAW) process, which has high productivity and high flexibility, and can be performed manually or automatically, thus making it one of the main processes used in industry. The GMAW process was done in accordance to Section IX, PART QW of the ASME Code (2007) [7]. The base material (type 304) was welded using 308LSi as filler material which is mechanically matched from the structural integrity point of view and which ensures corrosion resistance. The welds were done with an argon-based shielding gas, 98% Ar supplemented with 2 % CO₂, and a flow rate of 18 L/min. Two welding coupons were produced by the manufacturer to study the different types of full penetration joints performed for the CVBCS: a) a butt-welding coupon of 500 x 395 x 100 mm (longitudinal x transversal x thickness); b) a T-welding coupon of 34 mm thickness onto a 100 mm plate with overall dimensions of 500 mm (longitudinal direction), 200/34 mm (transversal), 34 mm thickness. See Fig. 4. The coupons

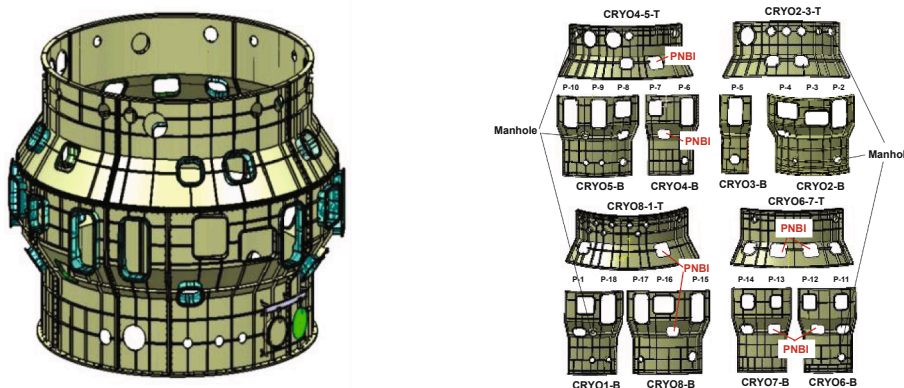


Fig. 3. Sketches of the CVBCS assembly (left) and the twelve sectors that form the CVBCS when divided into quadrants (right).

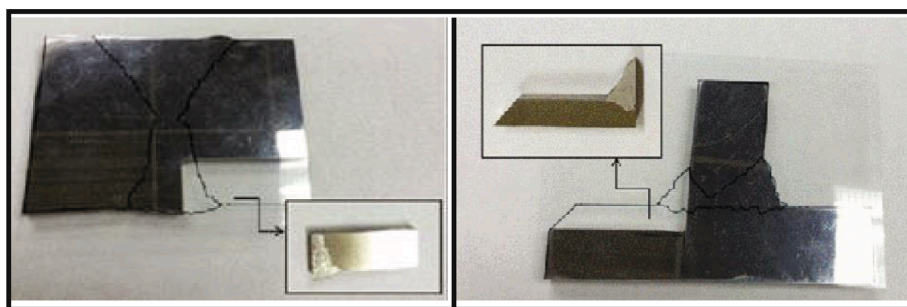


Fig. 4. Photos of samples obtained from the butt-welding (left) and T-welding (right) coupons produced with GMAW process for CVBCS.

Table 3
Chemical compositions for the base material and the filler metal.

	C %	Si %	Mn %	P %	Ni %	Cr %	N %	S %	Co %	Mo %	Cu %
Base metal	0.045	0.26	1.77	0.023	10.16	18.26	0.082	0.001	0.028	–	
Filler metal	0.02	0.80	1.9	0.02	10.5	19.9	0.05	0.01	0.04	0.13	0.07

Table 4
Welding parameters used for the welding coupons.

Base material	Filler material	Type- Polarity	Current range (I)	Voltage range (V)	Travel speed (cm/min)
UNS S30400	SFA 5.9 ER308LSi	DC EP	140–290	17,8–32	21,82–52,17

were extracted from a 100 mm thick plate.

The base material and the filler material composition contained very low levels of impurities such as phosphorus and sulphur, as they have a detrimental influence on the solidification cracking phenomena. In addition, a very low delta ferrite content (below 0.6%) for the base material was required. The chemical composition for the base material and filler metal is included in Table 3, whilst the welding parameters used are presented in Table 4. The following tests were conducted on specimens machined from the as-received coupons: a) Microstructural characterization, b) Hardness tests in transversal direction to the welds, c) Tensile tests in longitudinal (X) and transversal (Y, Z) directions (at RT and at -60 °C), d) Charpy tests in LT, LS and ST directions (at RT and at -196 °C). The experimental procedure conducted for the different tests was as follows: 1- Hardness: Vickers hardness was measured with an AKASHI AVK-AII durometer by applying 10 kg on the specimens. A mirror-polished surface finish was produced on the specimens. The samples prepared for these tests are shown in Fig. 5. 2- Mechanical tests were performed on standard and sub-size tensile specimens as shown in Fig. 6. The tensile tests were performed in LT, LS and ST directions at

two different temperatures, RT and -60 °C. Before testing, an exhaustive metrology control of the specimens was done. The applied standard was ASTM E8 / E8M - 09 Standard Test Methods for Tension Testing of Metallic Materials. A universal testing machine MTS 810 up to 100 kN was used. The deformation during the tests at RT was measured with an axial extensometer MTS, model 634.12F-21. Tests on the three orientations (L, T, S) were done with a total of 3 specimens per orientation and per temperature (RT / -60 °C). The cold tests were carried out in an environmental chamber with ± 2°C temperature control. For each specimen, a stabilization time of 10 min was used before performing the test. 3- Charpy impact tests were performed for both welding types, using sub-size Charpy specimens 10x5x55 mm. Tests for the three orientations (LT, LS and ST) were done with 3 specimens per orientation and per temperature (RT / -196 °C).

Results and Discussion

The microstructural characterization for the base material was done using optical microscopy. Heterogenic austenitic grains were observed

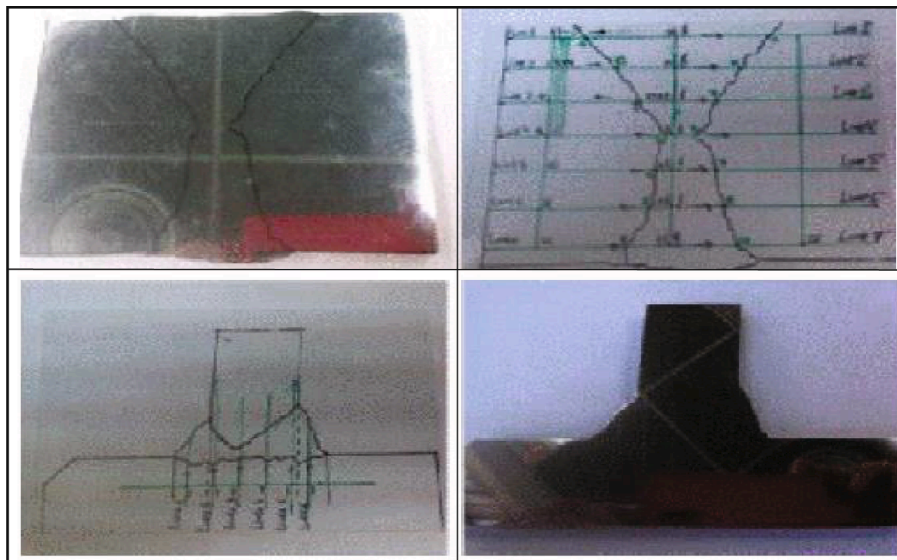


Fig. 5. Hardness measurements in the butt-welding coupon (upper) and the T-welding coupon (lower).

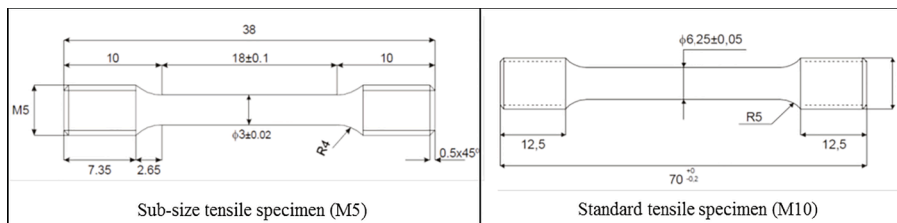


Fig. 6. Tensile specimens.

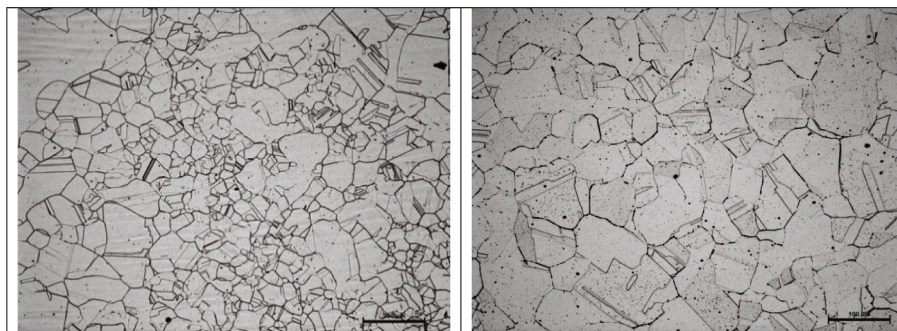


Fig. 7. CVBCS butt-welding coupon microstructure of the base material S30400.



Fig. 8. Microstructures in the HAZ (butt-welding coupon on the left and T-welding coupon on the right).

Table 5
Summary of the Vickers hardness measurements for the butt-welding coupon.

HARDNESS	LINE 1	LINE 2	LINE 3	LINE 4	LINE 5	LINE 6	LINE 7
MAX	203	222	211	247	222	233	215
MIN	154	135	137	123	123	116	134
μ	181.3	182.3	175.6	175	166	171.3	180.3
σ	10.4	24	26	35	33	36	24

Table 6
Summary of the Vickers hardness measurements for the T-welding coupon.

HARDNESS	LINE 1	LINE 2	LINE 3	LINE 4	LINE 5	LINE 6
MAX	196	194	218	207	199	195
MIN	134	148	140	148	152	152
μ	169.6	175.2	188	179.6	171.8	170.3
σ	17	13.3	23.5	20	16.2	14.3

as well as border grains precipitation with an average grain size corresponding to ASTM G=4. Some isolated grains presented large size (ASTM E-112 G=0). Due to the presence of carbides in the limit of the grains, an oxalic acid attack was performed as per ASTM A262-practice A (see Fig. 7). As a result, some of the grains showed a “ditch” structure,

i.e., with the whole perimeter attacked. The microstructure of the material in the Heat Affected Zone (HAZ) did not present microstructural changes (see Fig. 8). The microstructure of the filler material presented typical characteristics of the welding process –dendritic type– with columnar dendrites grains growing in the thermal gradient direction.

Vickers hardness measurements were done transversally to the weld along several lines. For the butt-welding coupon, 44 measurements per line were done with 2 mm distance between measurement points, while 22 measurements per line were done for the T-welding coupon. The measurements obtained per line for the different coupons are summarized in Tables 5 and 6 respectively. Maximum and minimum values as well as the mean value (μ) and the standard deviation (σ), are presented in the tables. All the measurements for both coupons resulted in higher values compared with the mean value obtained for the base material, i. e., 120. The butt-welding tensile tests were performed with the standard tensile specimens (M10) machined from the coupon provided by the manufacturer. Stress-strain curves for the three orientations at RT and $-60\text{ }^\circ\text{C}$ can be seen in Fig. 9. The T-welding tensile tests were performed with sub-size tensile specimens (M5) machined from the coupon provided by the manufacturer. The tests were done under the standard ASTM E8 / E8M - 09 Standard Test Methods for Tension Testing of Metallic Materials. The testing machine, the axial extensometer and the environmental chamber described in section 2 were used. Stress-strain

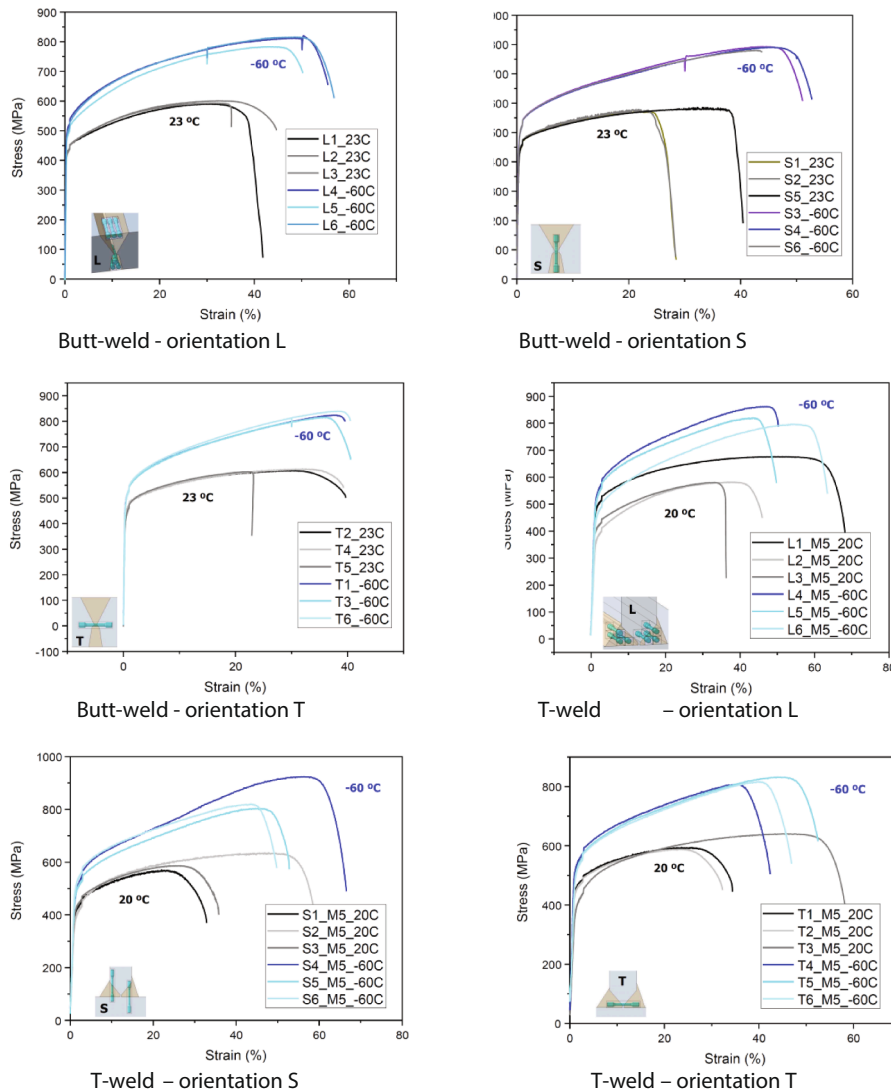


Fig. 9. Stress-strain curves for the butt-weld specimens (M10) and for the T-weld specimens (M5) in the 3 orientations performed at RT and $-60\text{ }^\circ\text{C}$.

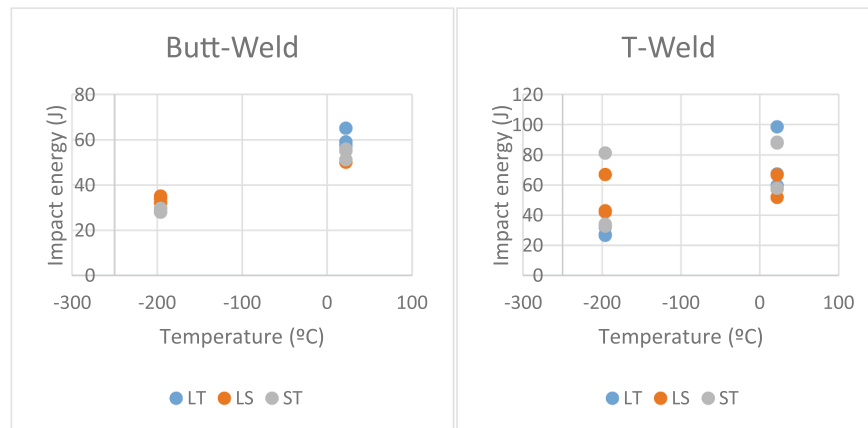


Fig. 10. Results of impact tests for the butt-weld and T-weld specimens.

curves for the different specimens in the three orientations at RT and -60°C can be seen also in the next Fig. 9.

Discussion

The microstructure analysis show typical characteristics for these types of steel and welds.

Hardness tests show higher values for the weld metal compared to the base metal. This result can be attributed to alloying elements of electrodes like chromium and molybdenum.

The tensile tests performed at RT do not show relevant differences (less than 5%) in the Yield strength and the Ultimate tensile strength tests when these values are compared for the three directions (L,T,S) per type of weld (butt/T welds). Additionally, when these results are compared for the two types of welds they are found to be quite similar (differences in the values are less than 4%).

The results of tensile tests performed down to -60°C showed a highly ductile behaviour of the material that presents as average (for the butt-welding in the rolling direction) up to 50% elongation, 494 MPa yield strength and 840 MPa ultimate tensile strength. When the yield strength of the welds and the base metal are compared, the results show higher values of the welds without a detrimental decrease in ductility. Finally, all the tensile specimens showed a ductile behaviour.

Impact tests performed down to -196°C showed impact energies above 20 J, this value being lower than values reported in the literature [8]. Scattering of the measurement for the different specimens was also found, as can be seen in Fig. 10 These results could be explained by the location of the notch (at the base material, HAZ or welds) in the different specimens.

Conclusions

- Within the CVBCS manufacturing phase, an extensive tests campaign was performed at Ciemat aimed at the characterization of the welds proposed by the manufacturer before their final approval: microstructure, hardness, tensile and impact tests were carried out as part of this validation process.
- From the microstructural characterization, the results are similar to those expected for this type of austenitic stainless steel 304. The material in the HAZ did not present microstructural changes. The microstructure of the filler material presented the typical characteristics of the welding process with columnar dendrites grain growth in the thermal gradient direction. From the microstructural characterization, the results are similar to those expected for this type of austenitic stainless steel 304. The material in the HAZ did not

present microstructural changes. The microstructure of the filler material presented the typical characteristics of the welding process with columnar dendrites grain growth in the thermal gradient direction.

- Hardness tests show higher values (m) for the weld metal compared with the mean value obtained for the base material.
- Tensile tests performed at RT and -60°C showed a highly ductile behaviour of the material.
- The yield strength of welds compared to the base material show higher values without a detrimental decrease in ductility.
- Results of impact tests at -196°C showed lower impact energies than expected.
- The global results showed satisfactory behaviour of the welds and no specific problems were identified.

CRediT authorship contribution statement

Mercedes Medrano: Conceptualization, Supervision, Writing – original draft. **Marta Serrano:** Investigation, Methodology, Writing – review & editing. **Rebeca Hernández:** Data curation, Validation, Visualization. **Daniel Plaza:** Resources. **Antonio Muñoz:** Resources. **Esther Rincón:** Writing – review & editing. **Santiago Cabrera:** Writing – review & editing. **Alfonso Soletto:** Writing – review & editing. **Augusto Pereira:** Writing – review & editing. **Cristina Alén:** Writing – review & editing.

Declaration of Competing Interest

The authors declare that they have no known competing financial interests or personal relationships that could have appeared to influence the work reported in this paper.

References

- [1] P. Barabaschi, et al., Nucl. Fusion 59 (2019), 112005, <https://doi.org/10.1088/1741-4326/ab03f6>.
- [2] E. Rincón, J. Alonso, G. Barrera, J. Botija, P. Fernández, M. Medrano, G. Pérez, F. Ramos, A. Soletto, P. Barabaschi, E. Di Pietro, L. Meunier, A. Sakasai, K. Masaki, Y. Shibama, Structural analysis of the JT-60SA cryostat base, Fusion Eng. Des. 86 (6–8) (2011) 623–626, <https://doi.org/10.1016/j.fusengdes.2011.01.008>.
- [3] J. Botija, J. Alonso, P. Fernández, M. Medrano, F. Ramos, E. Rincon, A. Soletto, S. Davis, E. Di Pietro, V. Tomarchio, K. Masaki, A. Sakasai, Y. Shibama, Structural analysis of the JT-60SA cryostat vessel body, Fusion Eng. Des. 88 (6–8) (2013) 670–674, <https://doi.org/10.1016/j.fusengdes.2013.02.120>.
- [4] M. Medrano, J. Alonso, J. Botija, P. Fernández, F. Ramos, E. Rincon, A. Soletto, S. Davis, E. Di Pietro, K. Masaki, A. Sakasai, Manufacturing of JT-60SA cryostat

- base, Fusion Eng. Des. 88 (6-8) (2013) 711–715, <https://doi.org/10.1016/j.fusengdes.2013.01.028>.
- [5] J. Botija, et al., Manufacturing of the JT-60SA cryostat vessel body cylindrical section, Fusion Eng. Des. 124 (2017) 537–541, <https://doi.org/10.1016/j.fusengdes.2017.04.055>.
- [6] ASTM A240/A240M; Standard Specification for Chromium and Chromium-Nickel Stainless Steel Plate, Sheet, and Strip for Pressure Vessels and for General Applications.
- [7] The American Society of Mechanical Engineers (ASME). 2007 ASME Boiler & Pressure Vessel Code. Section IX-Welding and Brazing Qualifications.
- [8] T. Ogawa, T. Koseki, Welding technology trend of austenitic stainless steels for cryogenic services, Yosetsu Gakkai-Shi 57 (6) (1988) 443–449.